Available online at www.sciencedirect.com

SciVerse ScienceDirect

journal homepage: www.elsevier.com/locate/ijrefrig

Numerical investigation of coupled heat and mass transfer inside the adsorbent bed of an adsorption cooling unit

İsmail Solmuş [a,*,1,2], D. Andrew S. Rees [b], Cemil Yamalı [a], Derek Baker [a], Bilgin Kaftanoğlu [c]

[a] Department of Mechanical Engineering, Middle East Technical University, 06531 Ankara, Turkey
[b] Department of Mechanical Engineering, University of Bath, Claverton Down, Bath BA2 7AY, UK
[c] Department of Manufacturing Engineering, Atılım University, 06836 Ankara, Turkey

ARTICLE INFO

Article history:
Received 14 April 2011
Received in revised form
13 December 2011
Accepted 14 December 2011
Available online 22 December 2011

Keywords:
Adsorption
Adsorbent
Cooling
Silica gel

ABSTRACT

In this study, the influence of several design parameters on the transient distributions of temperature, pressure and amount adsorbed in the radial direction of a cylindrical adsorbent bed of an adsorption cooling unit using silica gel/water have been investigated numerically. For this purpose, a transient one-dimensional local thermal non-equilibrium model that accounts for both internal and external mass transfer resistances has been developed using the local volume averaging method. For the conditions investigated, the validity of the local thermal equilibrium and spatially isobaric bed assumptions have been confirmed. To improve the performance of the bed considered, efforts should be focused on reducing heat transfer resistances and intra-particle (interior) mass transfer resistances but not inter-particle (exterior) mass transfer resistances.

© 2011 Elsevier Ltd and IIR. All rights reserved.

Etude numérique sur le transfert de chaleur et de masse à l'intérieur du lit absorbant d'un système de refroidissement à adsorption

Mots clés : Adsorption ; Adsorbant ; Refroidissement ; Gel de silice

1. Introduction

Thermally driven adsorption chillers (TDAC) have received much attention in the recent years since they are environmentally friendly and can be operated with low-grade heat sources such as solar energy or waste heat. However, these systems are not competitive with electrically-driven refrigeration systems due to their high investment costs and low coefficient of performance. Therefore, extensive efforts have been exerted by researchers to improve their

* *Corresponding author*. Tel.: +90 3122102563; fax: +90 3122102536.
E-mail address: solmus@metu.edu.tr (İ. Solmuş).
[1] Currently, visiting researcher at the Department of Mechanical Engineering, University of Bath, Claverton Down, Bath BA2 7AY, U.K.
[2] On leave of absence from Department of Mechanical Engineering, Atatürk University, 25240 Erzurum, Turkey.
0140-7007/$ – see front matter © 2011 Elsevier Ltd and IIR. All rights reserved.
doi:10.1016/j.ijrefrig.2011.12.006

Nomenclature

a_v	specific surface area, m^{-1}
c_p	heat capacity, J kg^{-1} K^{-1}
D_e	equivalent diffusivity in the adsorbent particles, m^2 s^{-1}
D_g	diffusivity of adsorbate gas, m^2 s^{-1}
D_k	Knudsen diffusivity, m^2 s^{-1}
D_m	molecular diffusivity, m^2 s^{-1}
D_o	reference diffusivity, m^2 s^{-1}
d_p	diameter of the adsorbent particle, m
d_{pore}	average pore diameter, m
E_a	activation energy of surface diffusion, J mol^{-1}
h_{gs}	interfacial heat transfer coefficient, W m^{-2} K^{-1}
K_a	apparent permeability, m^2
K_d	real permeability, m^2
K_E	inertial term, m
K_{g_e}	effective thermal conductivity for the gas phase, W m^{-1} K^{-1}
K_{s_e}	effective thermal conductivity for the solid phase, W m^{-1} K^{-1}
k_m	mass transfer coefficient within the adsorbent particles, s^{-1}
k	thermal conductivity, W m^{-1} K^{-1}
m	rate of refrigerant adsorbed unit control volume, kg_w m^{-3} s^{-1}
M	molar mass, kg mol^{-1}
Nu_d	Nusselt number
P	pressure, Pa
Pr	Prandtl number
Q	heat of adsorption, J Kg_w^{-1}
R	universal gas constant, J mol^{-1} K^{-1}
Re_d	Reynolds number
R_g	specific gas constant for water vapor, J kg^{-1} K^{-1}
r_i	inner diameter of the adsorbent bed, m
r_o	outer diameter of the adsorbent bed, m
r_p	radius of the adsorbent particle, m
T	temperature, K
t	time, s
v_r	velocity, m s^{-1}
X	adsorption capacity, $kg_w kg_{ad}^{-1}$
X_∞	amount adsorbed at equilibrium state, $kg_w kg_{ad}^{-1}$

Greek symbols

η	dynamic viscosity, N m^{-2}
ρ	density, kg m^{-3}
ε_t	total porosity
ε_b	bed porosity
ε_p	particle porosity
τ	tortuosity
σ	collision diameter for Lennard-Jones potential
Ω	collision integral

Subscripts

b	boundary
c	condenser
ev	evaporator
g	gas phase
h	regeneration
i	initial
s	solid phase
sat	saturation

coefficient of performance and make them commercially viable.

The successful operation of a TDAC system depends strongly on the performance of its adsorbent bed filled with a porous material. The performance of an adsorbent bed is affected adversely by the heat and mass transfer limitations inside the bed, such as poor thermal conductivity of the solid adsorbent, and internal (intra-particle) and external (inter-particle) mass transfer resistances. The internal and external mass transfer resistances are as the respective adsorbate gas flows inside the solid adsorbent particle and through the voids between the solid adsorbent particles. Over the past several decades, many researchers have proposed various mathematical models to investigate the heat or coupled heat and mass transfer mechanism inside the adsorbent beds of TDAC systems (Chahbani et al., 2002, 2004; Dai and Sumathy, 2003; Demir et al., 2009; Leong and Liu, 2004; Li and Wang, 2003; Maggio et al., 2006; Marletta et al., 2002; Mhimid, 1998; Wu et al., 2009; Zhang and Wang, 1999; Zhang, 2000). In these models, the equations have been developed for the heat transfer within a porous medium typically assuming a mobile gas (vapor) phase, an immobile solid phase (adsorbed adsorbate + adsorbent), and local thermal equilibrium between the gas and solid phases; the sole exception is the paper by Mhimid (1998). In the proposed conservation of mass equations, the mass transfer resistance within the solid adsorbent particles was typically accounted for and the internal mass transfer rate between the solid adsorbent and adsorbate gas phases (including sorption processes) was calculated using the solid diffusion (Chahbani et al., 2002) or linear driving force (Chahbani et al., 2002, 2004; Dai and Sumathy, 2003; Demir et al., 2009; Leong and Liu, 2004; Li and Wang, 2003; Maggio et al., 2006; Marletta et al., 2002; Mhimid, 1998; Wu et al., 2009; Zhang and Wang, 1999; Zhang, 2000) model. Darcy's law has been used widely to account for the external mass transfer through the voids between the solid adsorbent particles by convection (Dai and Sumathy, 2003; Demir et al., 2009; Leong and Liu, 2004; Mhimid, 1998; Wu et al., 2009; Zhang and Wang, 1999; Zhang, 2000). Additionally, in two instances the adsorbate gas velocity through the adsorbent bed was determined using Ergun's equation which includes inertial effects (Maggio et al., 2006; Marletta et al., 2002). On the other hand, in some previous studies, the pressure across the bed was assumed to be uniform as a result of a high permeability within the bed or the use of a high working-pressure refrigerant like ammonia (Chahbani et al., 2002, 2004; Li and Wang, 2003). Most of the previous studies, i.e. (Leong and Liu, 2004; Wu et al., 2009; Zhang and Wang, 1999; Zhang, 2000) and (Chahbani et al., 2002, 2004; Dai and Sumathy, 2003; Li and Wang, 2003; Maggio et al., 2006; Marletta et al., 2002), focused mainly on the effect of the heat and mass transfer limitations on the performance of the adsorption cooling systems in terms of COP and SCP, and only a two of studies, specifically (Demir et al., 2009) and (Mhimid,

1998), investigated the transient temperature and concentration distributions inside the adsorbent bed.

The objective of the present work is to investigate the coupled heat and mass transfer mechanisms inside the adsorbent bed of a solid sorption cooling unit during the adsorption process. For this purpose, a transient one-dimensional local thermal non-equilibrium model that accounts for both internal and external mass transfer resistances has been developed. In this model, it was assumed that significant temperature gradients exist between the vapor and solid adsorbent phases and hence, two different energy conservation equations are proposed to determine the separate temperature fields of the vapor and solid adsorbent phases; i.e., local thermal non-equilibrium was considered. The mathematical model developed in this study may be used to design and optimize a new and more efficient adsorbent bed.

2. Description of the adsorbent bed

A schematic of the cylindrical adsorbent bed under consideration is shown in Fig. 1. In this study, silica gel/water is used as an adsorbent-adsorbate working pair and their thermophysical properties are presented in Table 1. The bed consists of an inner vacuum tube, 36.5 mm in radius (r_o), a mass transfer tube, 9.5 mm in radius (r_i) and a larger tubular shell. The annulus between the vacuum and mass transfer tubes is filled with silica-gel granules. The vacuum tube is inserted into the larger tubular shell and cooled by a heat transfer fluid circulated between the shell and tube. Refrigerant vapor enters the vacuum tube through the top of the mass transfer tube and flows from the inner surface of the annulus to the annulus's outer surface. Both ends of the vacuum tube are well insulated and therefore heat and mass transfer are assumed to take place only in the radial direction.

3. Mathematical modeling

The system is modeled as consisting of vapor adsorbate, adsorbed adsorbate, and solid adsorbent, termed hereafter the vapor (or gaseous) phase, adsorbed phase, and adsorbent, respectively, for conciseness. The adsorbed phase is modeled as being immobile and in thermal equilibrium with the adsorbent, and its volume fraction is assumed negligible. The combination of the adsorbed phase and adsorbent are modeled as a single solid and are referred to collectively as the solid phase. The resulting model is therefore two-phase (vapor and solid) with single phase flow (vapor).

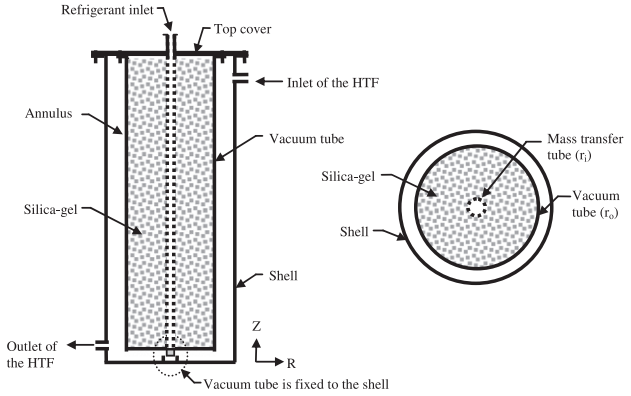

Fig. 1 – A schematic view of the cylindrical adsorbent bed.

Table 1 – Main simulation parameters.

Parameter	Reference	Value	Unit
ε_b	Chua et al., 2004	0.37	–
ε_p	Chua et al., 2004	0.42	–
d_p	Demir et al., 2009	$3.2e^{-3}$	m
μ_g	Maggio et al., 2006	$1.5e^{-5}$	$kgm^{-1}s^{-1}$
ρ_s	Demir et al., 2009	670	kgm^{-3}
c_{ps}	Demir et al., 2009	880	$Jkg^{-1}K^{-1}$
c_{pg}	Mhimid, 1998	1840	$Jkg^{-1}K^{-1}$
D_o	Di et al., 2007	$2.54e^{-4}$	$m^2\ s^{-1}$
E_a	Di et al., 2007	$4.2e^{4}$	$Jmol^{-1}$
k_g	Demir et al., 2009	0.0196	$Wm^{-1}K^{-1}$
k_s	Demir et al., 2009	0.198	$Wm^{-1}K^{-1}$
σ	Demir et al., 2009	2.641	A
Ω	Demir et al., 2009	2.236	–
d_{pore}	Demir et al., 2009	$2e^{-9}$	m
τ	Demir et al., 2009	3	–
r_o	–	36.5	mm
r_i	–	9.5	mm
P_{ev}	–	1.228	kPa
T_b	–	30	°C
T_h	–	120	°C
P_c	–	4.246	kPa

In the present study, the local volume averaging method, which has been utilized extensively in developing models for transport processes in porous media, was used to derive the governing macroscopic conservation equations from the microscopic ones. The details of this method are found in references (Duval et al., 2004; Nield and Bejan, 1999; Sözen and Vafai, 1990; Hager et al., 2000).

The model is primarily based on the assumptions and simplifications presented as follows:

- the size of the adsorbent particles and the bed porosity are spatially uniform;
- the adsorbate's vapor phase is assumed to be an ideal gas;
- radiative heat transfer, viscous dissipation and the work done by pressure changes are neglected;
- the surface porosity is considered to be equal to the total porosity;
- physical properties such as thermal conductivities, specific heat capacities and viscosity are not a function of temperature;
- the wall thickness of the vacuum tube is assumed to be very thin and hence, its thermal resistance is neglected.

3.1. Mass conservation equation

The macro scale mass conservation equation for the adsorbate gas can be written as:

$$\varepsilon_t \frac{\partial(\rho_g)}{\partial t} + \frac{1}{r}\frac{\partial(r\rho_g v_r)}{\partial r} + \dot{m} = 0 \quad (1)$$

The rate of the amount of refrigerant adsorbed in Eq. (1) is defined as:

$$\dot{m} = (1-\varepsilon_t)\rho_s \frac{\partial X}{\partial t} \tag{2}$$

The volume fraction of the gas phase, ε_g is assumed to be equal to the total porosity, ε_t, and may be evaluated using (Zhang, 2000),

$$\varepsilon_t = \varepsilon_b + (1-\varepsilon_b)\varepsilon_p \tag{3}$$

The mass transfer resistance within the adsorbent particles is taken into account, i.e., adsorption equilibrium is not assumed. The Linear Driving Force (LDF) model is used to describe the adsorption rate or internal mass transfer (Di et al., 2007). The LDF model is expressed as follows:

$$\frac{\partial X}{\partial t} = k_m(X_\infty - X) \tag{4}$$

where k_m is the internal mass transfer coefficient given by

$$k_m = 15D_e/r_p^2 \tag{5}$$

and D_e is the equivalent diffusivity in the adsorbent particles which may be expressed as (Di et al., 2007)

$$D_e = D_o \exp(-E_a/RT_s) \tag{6}$$

The equilibrium adsorption capacity of the silica gel/water pair was evaluated using the following modified Dubinin-Astakhov (D-A) equation (Di et al., 2007).

$$X_\infty = 0.346\exp\left[-5.6(T_s/T_{sat}-1)^{1.6}\right] \tag{7}$$

3.2. Momentum equation

The velocity of the adsorbate gas in the radial direction is determined by using the following Ergun's equation (Marletta et al., 2002). This equation is more general than Darcy's equation since it not only includes viscous effects but also inertial effects. Ergun's equation is,

$$v + \frac{\rho_g}{\eta_g}K_E v|v| = -\frac{K_a}{\eta_g}\nabla P \tag{8}$$

The parameter, K_E, which is usually called the Forchheimer coefficient, that appears in Ergun's equation accounts for the inertial effects and is defined as follows:

$$K_E = \frac{1.75d_p}{150\cdot(1-\varepsilon_b)} \tag{9}$$

The parameter K_a is the apparent permeability that takes into account diffusion and viscous flow, and described in (Maggio et al., 2006) as:

$$K_a = K_d + \frac{D_g\eta_g}{P} \tag{10}$$

where K_d is the real permeability which can be calculated by the following the semi-empirical Blake-Kozeny equation,

$$K_d = \frac{d_p^2\varepsilon_b^3}{150(1-\varepsilon_b)^2} \tag{11}$$

The diffusivity of the adsorbate gas D_g, which involves Knudsen and molecular diffusions, was evaluated by the following relation (Marletta et al., 2002; Karger and Rutheven, 1992)

$$D_g = \left(\frac{1}{D_m}+\frac{1}{D_k}\right)^{-1}\frac{\varepsilon_b}{\tau} \tag{12}$$

where, $D_m = 0.02628\sqrt{T^3/M}/P\sigma^2\Omega$ and $D_k = 48.5d_{pore}(T/M)^{0.5}$

3.3. Energy conservation equations

Two different energy conservation equations are developed to determine the separate temperature fields of the gas and solid adsorbent phases; i.e., local thermal equilibrium was not assumed.

3.3.1. Energy conservation equation for the gas phase

The macro scale energy conservation equation for the gas phase is written as:

$$c_{pg}\rho_g\left[\varepsilon_t\frac{\partial T_g}{\partial t} + v_r\frac{\partial T_g}{\partial r}\right] + (1-\varepsilon_t)\rho_s\frac{\partial X}{\partial t}c_{pg}(T_s - T_g) = \frac{1}{r}\frac{\partial}{\partial r}\left(rK_{g\_e}\frac{\partial T_g}{\partial r}\right) + a_v h_{gs}(T_s - T_g) \tag{13}$$

3.3.2. Energy conservation equation for the solid phase

The local volume-averaged macroscopic energy conservation equation for the solid phase is given by

$$\rho_s(1-\varepsilon_t)\left[c_{ps} + Xc_{pg}\right]\frac{\partial T_s}{\partial t} = \frac{1}{r}\frac{\partial}{\partial r}\left(rK_{s\_e}\frac{\partial T_s}{\partial r}\right) - a_v h_{gs}(T_s - T_g) + (1-\varepsilon_t)\rho_s\frac{\partial X}{\partial t}Q \tag{14}$$

The effective thermal conductivity for the solid and gas phases can be defined as follow (Nield and Bejan, 1999)

$$K_{s\_e} = k_s(1-\varepsilon_t) \text{ and } K_{g\_e} = k_g\varepsilon_t \tag{15}$$

The vapor–solid specific surface area for spherical particles is determined by (Mhimid, 1998)

$$a_v = 6(1-\varepsilon_t)/d_p \tag{16}$$

The interfacial heat transfer coefficient for the spherical particle is evaluated by (Mhimid, 1998)

$$Nu_d = 2 + 1.8Pr^{0.33}Re_d^{0.5} \tag{17}$$

where, $Re_d = \rho_g v_r d_p/\eta_g$, $Nu_d = h_{gs}d_p/k_g$, $Pr = \eta_g c_{pg}/k_g$.

The isosteric heat of adsorption (Q) for the silica-gel/water working pair is determined by using the following equations (Rady et al., 2008)

$$\begin{aligned} Q &= 3500 - 13400X \quad \text{for } X \le 0.05 \\ Q &= 2950 - 1400X \quad \text{for } X > 0.05 \end{aligned} \tag{18}$$

The equation of state for the adsorbate vapor phase is written as:

$$P = \rho_g R_g T_g \tag{19}$$

3.4. Initial and boundary conditions

The temperatures (solid and gas), pressure and amount-adsorbed distributions in the radial direction inside the adsorbent bed are initially considered to be uniform.

$$T_g(0,r) = T_s(0,r) = T_i; \quad P(0,r) = P_i; \quad X(0,r) = X_i \tag{20}$$

At the inner surface of the annulus, it is assumed that the adsorbate gas pressure is equal to the evaporator pressure,

and the temperature gradients for both the solid and gas phases are zero.

$$P(t,R_i)=P_e,\quad \frac{\partial T_g}{\partial r}(t,R_i)=\frac{\partial T_s}{\partial r}(t,R_i)=0 \tag{21}$$

At the solid wall (i.e. the outer surface of the annulus), there is a zero pressure gradient because the wall is impermeable, and the temperatures of the solid and gas phases are equal to a prescribed boundary temperature. Moreover, there is local thermal equilibrium between the phases at this boundary.

$$\frac{\partial P}{\partial r}(t,R_o)=0,\quad T_g(t,R_o)=T_s(t,R_o)=T_b \tag{22}$$

4. Solution procedure

The coupled governing partial differential equations were solved numerically due to their complexity and nonlinearity. The finite difference technique was used to convert these equations to a system of algebraic equations and a fully implicit scheme was chosen to eliminate possible numerical instabilities. The unsteady, diffusion, and convective terms were discretized using forward difference, central difference, and first order upwind schemes, respectively. The Newton–Raphson iteration scheme and a block tridiagonal matrix algorithm (Thomas algorithm) were employed to solve the resulting highly nonlinear algebraic equations iteratively. Thirty five grid points in the radial direction and a 5 s time step were chosen and these values were checked in terms of numerical accuracy. A computer simulation program based on the numerical procedure above was written in Matlab to perform the parametric investigation. In the simulation program, at each time step, iterations were terminated when the calculated difference between two successive iterations of any dependent variable was less than 10^{-6}. The main simulation parameters used in the computer simulation program are given in Table 1.

The initial temperatures for the gas and solid phases were calculated by means of the generation (hot) temperature of the adsorbent bed (T_h), condenser pressure (P_c), and evaporator pressure (P_{ev}). The adsorption capacity of the solid adsorbent was assumed to be constant as the pressure inside the adsorbent bed was decreased from the condenser to the evaporator pressure.

5. Results and discussion

The parameters studied such as adsorbent particle diameter, which is related to adsorbent density, and total porosity are mutually dependent variables and hence therefore one cannot be held constant while the other is varied. However, in this work as a first approximation the adsorbent particle diameter and total porosity are assumed to be independent. Moreover, the thermal conductivity of the solid adsorbent material (but not effective thermal conductivity) was varied by considering the adsorbent material to have various thermal conductivity values. It was also considered that the density of the solid adsorbent bed is constant and thus, the mass of the solid adsorbent inside the bed varies when the volume or thickness of the vessel is changed and this affects the amount of refrigerant adsorbed by the adsorbent material.

In general, the pressure distribution for each case of the parameter investigated is presented in the same figure due to nearly uniform pressure distributions. The colors of the lines in the temperature diagrams represent the locations inside the adsorbent bed and these representations are also valid for the pressure diagrams. In the pressure diagrams, pressure distribution for each case is represented by different line styles and they are presented in the captions of the figures.

5.1. *Temperature difference between the solid and gas phases*

One of the main objectives of this study is to investigate the validity of the single energy equation model that results from local thermal equilibrium assumption. Transient temperature differences between the solid and gas phases in the radial direction are illustrated in Fig. 2. For each plot in Fig. 2, all parameters except for that given in the plot are equal to the base case values. Generally, the temperature difference between the two phases is negligibly small for all cases investigated. However, it may need to be taken into account in the early stages of the process. It is obvious in Fig. 2 that, initially, there is a large temperature difference between the two phases near the outer boundary but not in the rest of the bed. However, this temperature difference decreases near the outer boundary and slightly increases in the rest of the bed up to a certain point in time and then it decreases gradually throughout the bed as time progresses. As a result, the temperature difference between the phases become less than 0.5 K when the time is equal to 1860, 1680, 780 and 420 s for deviations from the base case conditions as $\varepsilon_t = 0.826$, $d_p = 8$ mm, $k_s = 0.1$ Wm^{-1} K^{-1} and $r_o - r_i = 13.5$ mm, respectively.

5.2. *Adsorbent particle diameter*

The effect of the diameter of the adsorbent particles ($d_p = 8$ mm, $d_p = 4$ mm and $d_p = 2$ mm) on the transient solid and gas phase temperatures and pressure for the case are presented in Fig. 3. The values for all parameters except d_p are equal to their base case values given in Table 1. It can be seen from Fig. 3 that the diameter of the adsorbent particles exerts considerable influence on the transient temperature distributions but only a slight influence on the pressure distribution under the given conditions. The temperature difference between the outer and inner boundaries decreases with time and this difference is comparatively high for the $d_p = 2$ mm case at the beginning of the process. As the particle diameter increases, the internal mass transfer resistances increases, and the adsorption rate decreases. Consequently, the rate of heat release decreases and this leads to a decrease in the temperature difference between the outer and inner boundaries of the bed as well. In addition, this temperature difference becomes less than 5 °C for times greater than 3900, 17,460 and 13,500 s for particle diameter of 8, 4 and 2 mm, respectively. The uniform pressure assumption is valid for all cases considered, especially when the particle diameter is greater than 2 mm.

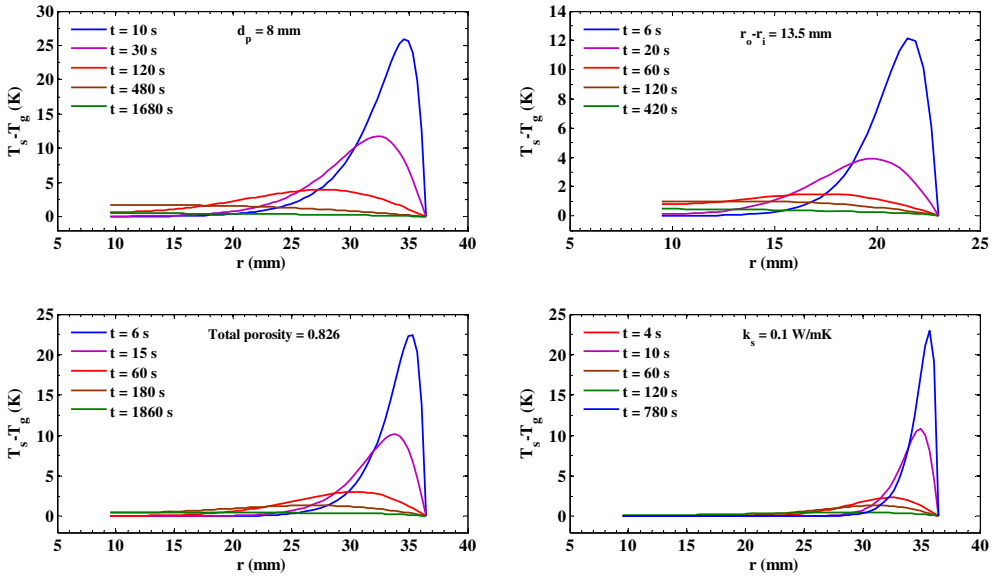

Fig. 2 – Transient temperature differences between solid and gas phases. All parameters assume the base case values in Table 1 except those indicated in each plot.

Transient distributions of the amount adsorbed calculated using the equilibrium and LDF models through the bed for $d_p = 8$ mm, $d_p = 4$ mm and $d_p = 2$ mm are illustrated in Fig. 4. It is obvious that the difference in the amount adsorbed between the equilibrium and LDF models decreases with decreasing particle diameter. The reason behind this behavior is that the internal mass transfer coefficient increases when the particle diameter is decreased and this causes an increase in the rate of adsorption according to the LDF model. In addition, the gradient in the amount adsorbed across the bed for both models increases with the decreasing particle diameter. As a result, if the particle diameter is greater than 2 mm the use of the equilibrium model may lead to an overestimate in the amount adsorbed by the adsorbent bed. However, even when the particle diameter is equal to 2 mm, there can still be large difference between the two models, especially near the outer boundary where the internal mass transfer coefficient is comparatively low due to low temperatures.

5.3. *Adsorbent bed thickness*

It is considered that the density of the solid adsorbent bed is constant and thus, the mass of the solid adsorbent inside the bed varies when the volume of the vessel is changed. The porosity of the adsorbent bed and the density of the solid

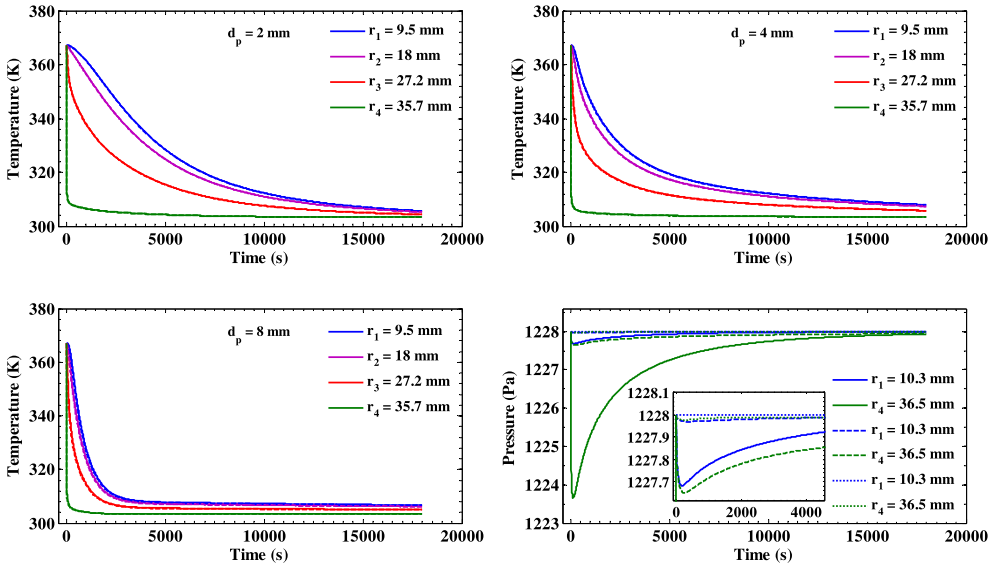

Fig. 3 – Transient temperature of solid and gas phase and pressure distributions for various adsorbent particle diameters. (Temperature: solid lines = T_s; dashed lines = T_g. Pressure: solid lines for $d_p = 2$ mm; dashed lines for $d_p = 4$ mm; and, square dots $d_p = 8$ mm).

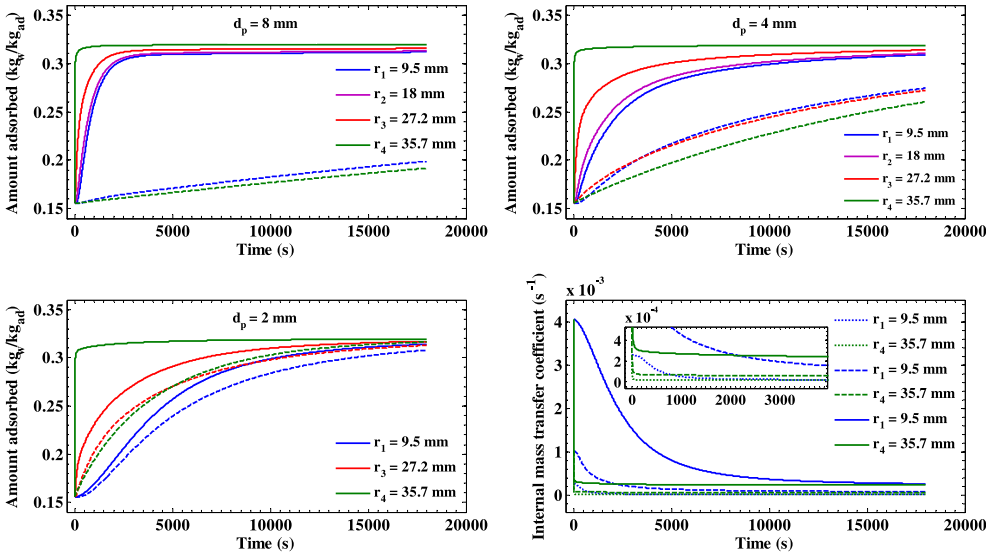

Fig. 4 – Transient amount adsorbed and internal mass transfer coefficient distributions for various adsorbent particle diameters (Amount adsorbed: solid lines = X_∞; dashed lines = X. Internal mass transfer coefficient: solid lines for d_p = 2 mm; dashed lines for d_p = 4 mm; and, square dots for d_p = 8 mm).

adsorbent are not affected by the variation of the adsorbent bed radius due to constant value of the density of the adsorbent material. However, this is not valid for the mass of solid adsorbent and pressure drop inside the adsorbent bed.

The temperatures of the solid and gas phases, the pressure, the amount adsorbed, and the internal mass transfer coefficient in the radial direction have been investigated for adsorbent bed thicknesses of 13.5, 27 (base case) and 54 mm, and the results are presented in Figs. 5 and 6. It is shown in Fig. 5 that the temperature distributions inside the bed become almost uniform after 4800 and 15,900 s for the 13.5 and 27 mm bed thicknesses, respectively. However, the adsorbent bed having a 54 mm bed thickness needs more than 28,800 s to reach a uniform temperature distribution. It may be concluded that the heat transfer in the radial direction can be enhanced by decreasing the adsorbent bed thickness. For the conditions investigated, external mass transfer resistances do not result in significant pressure gradients and hence they may be ignored and a uniform pressure distribution throughout the bed can be assumed.

The transient distribution of the amount adsorbed has been evaluated using the equilibrium and LDF models for 54,

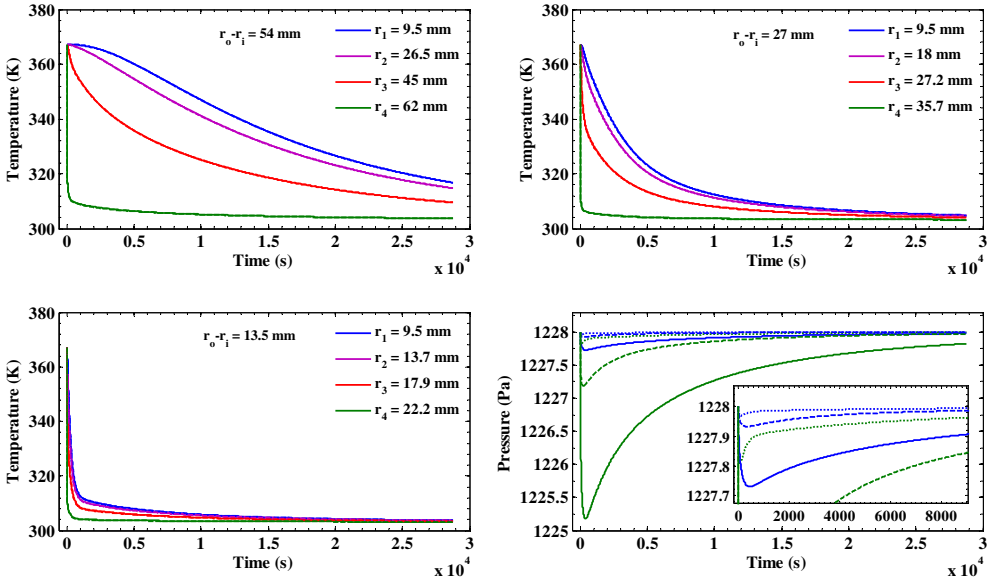

Fig. 5 – Transient temperature of solid and gas phase and pressure distributions for various adsorbent bed thicknesses (Temperature: solid lines = T_s; dashed lines = T_g. Pressure with same locations as the temperatures: solid lines for $r_o - r_i$ = 54 mm; dashed lines for $r_o - r_i$ = 27 mm; and, square dots for $r_o - r_i$ = 13.5 mm).

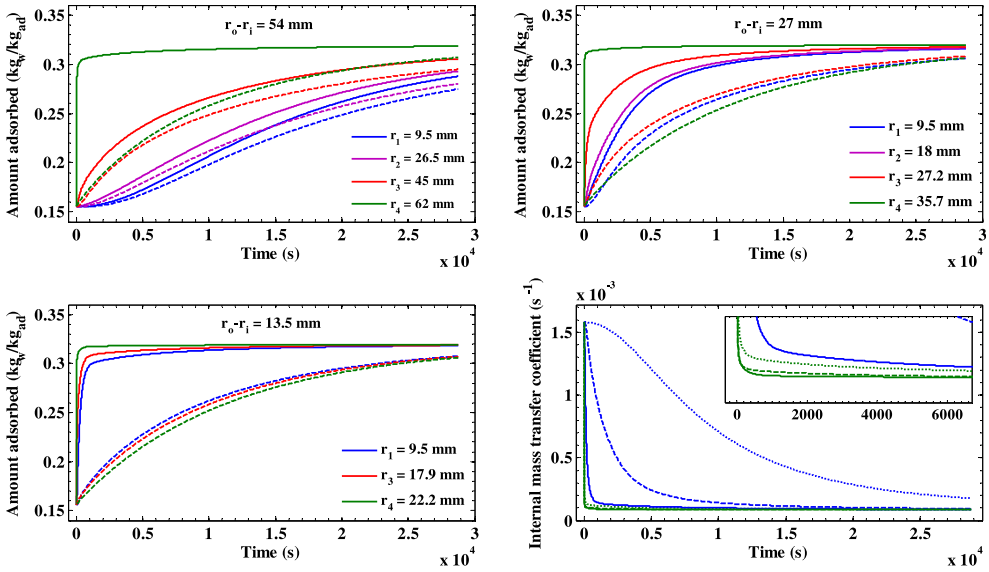

Fig. 6 – Transient amount adsorbed and internal mass transfer coefficient distributions for various adsorbent bed thicknesses (Amount adsorbed: solid lines X_∞; dashed lines X. Internal mass transfer coefficient at same locations as temperature: solid lines for $r_o - r_i = 13.5$ mm; dashed lines for $r_o - r_i = 27$ mm; and, square dots for $r_o - r_i = 54$ mm).

27 and 13.5 mm bed thicknesses. It can be seen from Fig. 6 that, for the 27 and 13.5 mm bed thicknesses, the difference in amount adsorbed between the two models at various locations in the bed decreases as the process time increases and this difference becomes less than 0.02 kg_w/kg_{ad} after 28,800 s; i.e. the adsorbent bed nearly reaches its equilibrium adsorption capacity. However, this difference increases slightly with increasing process time near the inner boundary of the bed having 54 mm bed thickness, which can be explained as follows. Initially, the two models give similar results near the inner boundary. However, when the temperature starts to decrease, the equilibrium adsorption capacity increases and the internal mass transfer coefficient decreases. As a result, the difference in rates of adsorption between the two models increases slightly. The transient distribution of amount adsorbed inside the bed for the LDF model becomes nearly uniform when the adsorbent bed thickness is decreased. It is clear in Fig. 5 that, when the adsorbent bed thickness is decreased, the transient temperature and pressure distributions inside the bed become almost uniform in a short period of time and hence, equilibrium adsorption capacity as well. On the other hand, the LDF model is related to the equilibrium adsorption capacity and the internal mass transfer coefficient. At the same time, the internal mass transfer coefficient only varies with temperature for this case and it decreases with a decreasing temperature. As a result, the internal mass transfer coefficient and the equilibrium adsorption capacity are uniform and thus the LDF model predicts a uniform distribution of amount adsorbed when the adsorbent bed thickness is small. For large bed thicknesses the response of the bed is limited by external (inter-particle) heat transfer resistances and adsorption equilibrium can be assumed at the particle level. However, for small bed thickness the response of the bed is limited by internal (intra-particle) mass transfer resistances and adsorption equilibrium cannot be assumed at the particle level. Finally, if the adsorbent bed thickness is less than 54 mm, then the use of the equilibrium adsorption model instead of the LDF model may lead to unrealistic simulation results. However, the equilibrium adsorption model may also exhibit large simulation errors near the outer boundary as the adsorbent bed thickness is greater than 54 mm for the given boundary conditions.

5.4. *Total porosity*

The transient variation of the temperatures, the pressure and the amount adsorbed in the radial direction for three different values of the total porosity are shown in Fig. 7 and Fig. 8. It can be seen from Fig. 7 that adsorbent beds having a porosity of $\varepsilon_t = 0.478$, $\varepsilon_t = 0.652$ and $\varepsilon_t = 0.826$ reaches a uniform temperature distribution (i.e the maximum temperature difference between the inner and outer boundaries is less than 4.5 °C) when the process time is equal to 18,000, 16,560, and 14,160 s, respectively. It can be concluded that the heat transfer conditions inside adsorbent bed are positively affected if the total porosity is increased. The external mass transfer resistance increases strongly as the total porosity of the bed is decreased. Therefore, the external mass transfer resistance should be considered for this problem when the total porosity of the adsorbent bed is less than 0.652 or the bed permeability is less than the order of 10^{-8}.

The total porosity of the adsorbent bed over the range investigated has only a small effect on the transient distribution of amount adsorbed for the equilibrium and LDF models. The adsorption rate predicted by the equilibrium model decreases with decreasing total bed porosity due to the increasing importance of external mass transfer resistances. According to the LDF model, internal mass transfer

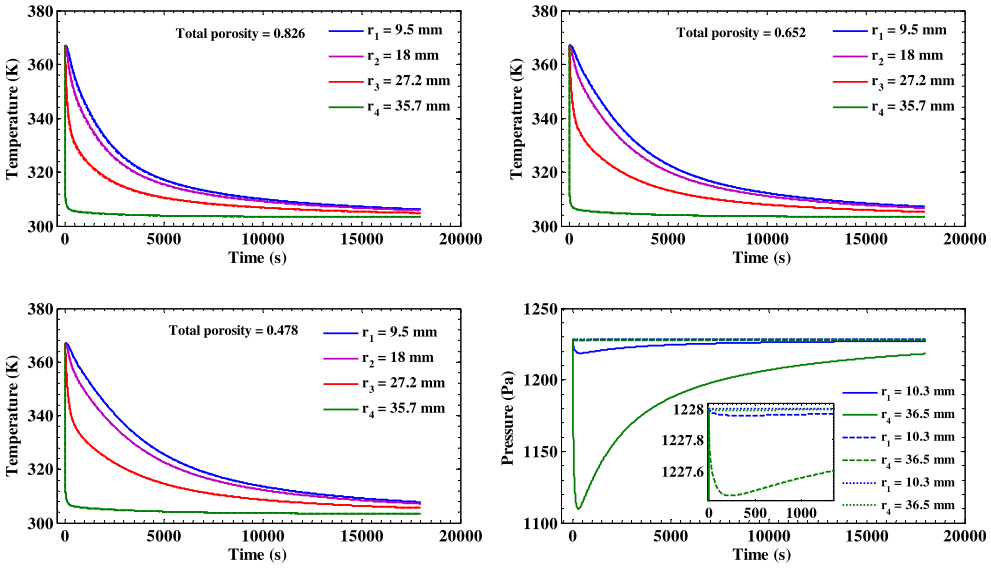

Fig. 7 – Transient temperature of solid and gas phase and pressure distributions for various total porosities of the adsorbent bed (Temperature: solid lines = T_s; dashed lines = T_g. Pressure: solid lines for $\varepsilon_t = 0.478$; dashed lines for $\varepsilon_t = 0.652$; and square dots for $\varepsilon_t = 0.826$).

resistances are large relative to external mass transfer resistances, and therefore adsorption rates are relatively insensitive to changes in total bed porosity if the particle porosity is held constant. As result, the difference between these two models decreases as the total bed porosity decreases. However, for all cases investigated the difference between these two models is still high and thus internal mass transfer resistances should be taken into account.

5.5. *Thermal conductivity of the solid phase*

The effect of the thermal conductivity of the solid phase on the transient distributions of the temperatures and the amount adsorbed is shown in Fig. 9 and Fig. 10, respectively. The heat transfer rate inside the adsorbent bed is influenced strongly by the solid phase thermal conductivity. It is very obvious in Fig. 9 that after 600 s the temperature difference

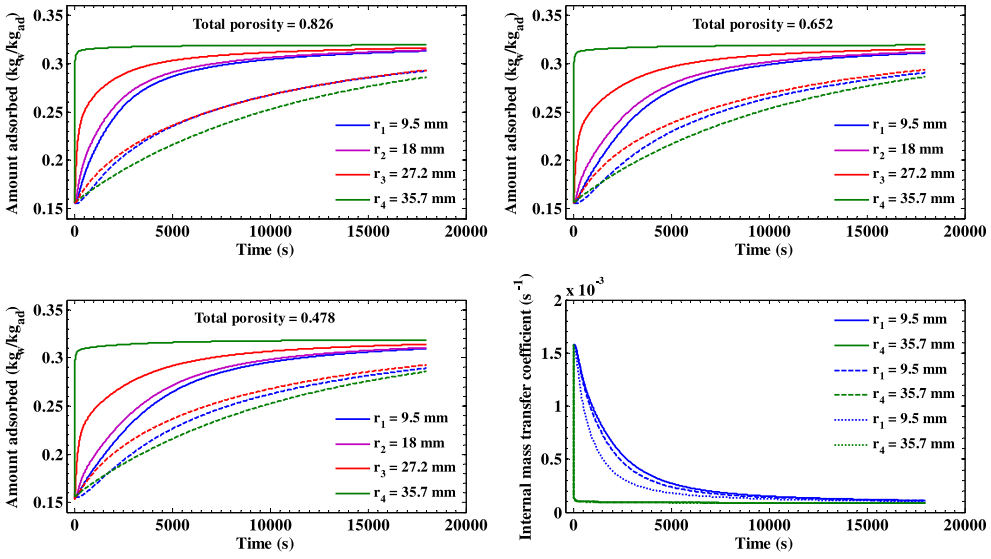

Fig. 8 – Transient amount adsorbed and internal mass transfer coefficient distributions for various adsorbent bed porosities (Amount adsorbed: solid lines = X_∞; dashed lines = X. Internal mass transfer coefficient: solid lines for $\varepsilon_t = 0.478$; dashed lines for $\varepsilon_t = 0.652$; and square dots for $\varepsilon_t = 0.826$).

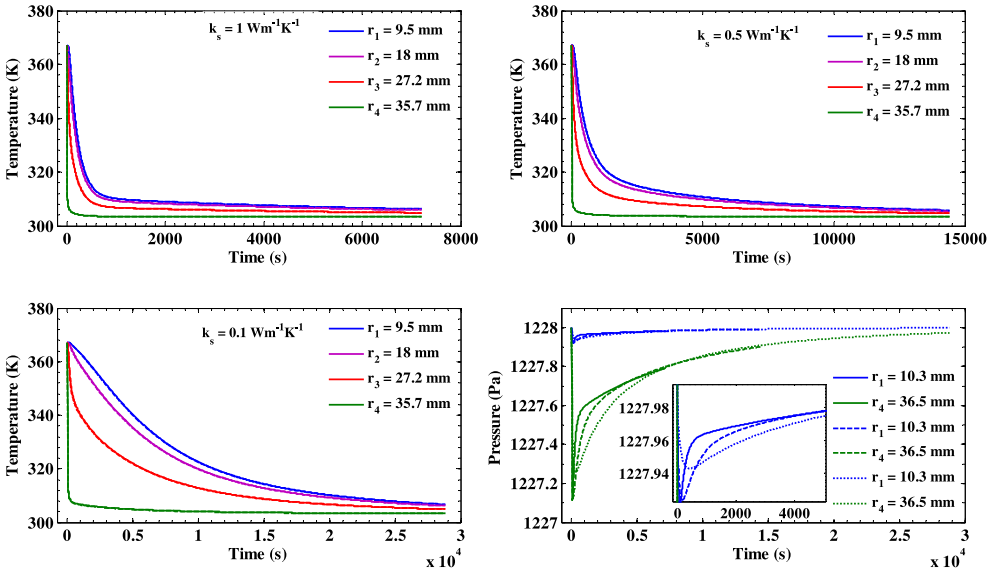

Fig. 9 – Transient temperature of solid and gas phase and pressure distributions for various thermal conductivity of the adsorbent material (Temperature: solid lines = T_s; dashed lines = T_g. Pressure: solid lines for k_s = 1 $Wm^{-1}K^{-1}$; dashed lines for k_s = 0.5 $Wm^{-1}K^{-1}$; and square dots for k_s = 0.1 $Wm^{-1}K^{-1}$).

between the inner and outer boundaries of the bed is less than 10 °C when $k_s = 1\ Wm^{-1}K^{-1}$. However, this time becomes 3300 and 16,200 s when $k_s = 0.5\ Wm^{-1}K^{-1}$and $k_s = 0.1\ Wm^{-1}K^{-1}$, respectively. Therefore the heat transfer conditions of the bed can be improved considerably by reducing heat transfer resistances through the use of fins, highly conductive adsorbent materials or other heat transfer enhancement techniques. The pressure distributions for all cases are nearly uniform and thus the uniform pressure assumption is valid.

In Fig. 10, the amount adsorbed calculated using the equilibrium adsorption model increases sharply to a maximum value (at T_b and P_{ev}) in a short period of time for k_s = 1 $Wm^{-1}K^{-1}$ due to the high heat transfer rate and negligible pressure gradients. On the other hand, the adsorption rate for the LDF model is very slow due to the internal mass transfer resistances. Therefore, initially, there is a big difference between the equilibrium adsorption and LDF models and this difference decreases as time increases. In addition, the difference in the amount adsorbed between the two models decreases with decreasing thermal conductivity. However, this difference remains large near the outer boundary at the beginning of the process.

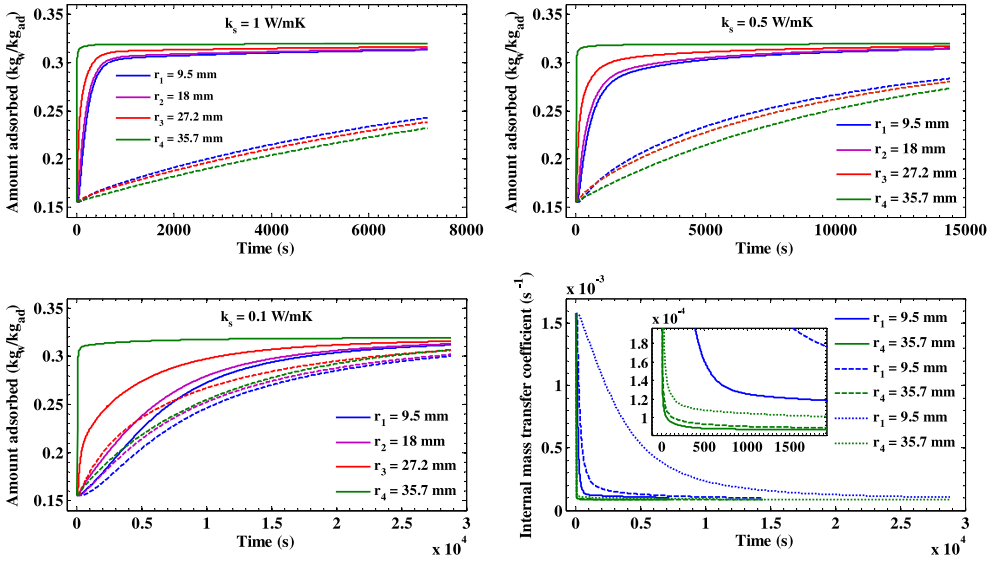

Fig. 10 – Transient amount adsorbed and internal mass transfer coefficient distributions for various thermal conductivity of the adsorbent material (Amount adsorbed: solid lines = X_∞; dashed lines = X. Internal mass transfer coefficient: solid lines for k_s = 1 $Wm^{-1}K^{-1}$; dashed lines for k_s = 0.5 $Wm^{-1}K^{-1}$; and square dots for k_s = 0.1 $Wm^{-1}K^{-1}$).

6. Conclusions

In this application an ideal adsorbent bed is always at thermal, mechanical and chemical equilibrium. The deviation of the bed from thermal, mechanical or chemical equilibrium, or the time required to reach thermal, mechanical and chemical equilibrium, is a measure of the opportunity to improve the performance of the bed through better design. In this model, the deviations from thermal, mechanical, and chemical equilibrium scale with heat transfer, external (inter-particle) mass transfer, and internal (intra-particle) mass transfer resistances. The length scales associated with the heat transfer and external mass transfer resistances are on the order of the radius of the adsorbent bed while that associated with the internal mass transfer resistance is on the order of the particle diameter.

Significant spatial temperature and pressure gradients indicate that heat transfer and external mass transfer resistance are important, while significant deviations of the amount adsorbed from the equilibrium amount adsorbed indicate that internal mass transfer resistances are important. To improve the performance of the bed, effort should be focused on reducing any significant resistances.

Acknowledgment

Ismail Solmus would like to thank The Scientific & Technological Research Council of Turkey (TÜBİTAK) and the Middle East Technical University for supporting him with a fellowship during his study at the University of Bath in the United Kingdom.

REFERENCES

Chahbani, M.H., Labidi, J., Paris, J., 2002. Effect of mass transfer kinetics on the performance of adsorptive heat pump systems. Appl. Therm. Eng. 22, 23–40.

Chahbani, M.H., Labidi, J., Paris, J., 2004. Modeling of adsorption heat pumps with heat regeneration. Appl. Therm. Eng. 24, 431–447.

Chua, H.T., Ng, K.C., Wang, W., Yap, C., Wang, X.L., 2004. Transient modeling of a two-bed silica gel–water adsorption chiller. Int. J. Heat Mass Tran. 47, 659–669.

Dai, Y.J., Sumathy, K., 2003. Heat and mass transfer in the adsorbent of a solar adsorption cooling system with glass tube insulation. Energy 28, 1511–1527.

Demir, H., Mobedi, M., Ülkü, S., 2009. Effect of porosity on heat and mass transfer in a granular adsorbent bed. Int. Commun. Heat Mass Transf. 36, 372–377.

Di, J., Wu, J.Y., Xia, Z.Z., Wang, R.Z., 2007. Theoretical and experimental study on characteristics of a novel silica gel-water chiller under the conditions of variable heat source temperature. Int. J. Refrig. 30, 515–526.

Duval, F., Fichot, F., Quintard, M., 2004. A local thermal non-equilibrium model for two-phase flows with phase-change in porous media. Int. J. Heat Mass Tran. 47, 613–639.

Hager, J., Wimmerstedt, R., Whitaker, S., 2000. Steam drying a bed of porous spheres: theory and experiment. Chem. Eng. Sci. 55, 1675–1698.

Karger, J., Rutheven, M.D., 1992. Diffusion in Zeolites and Other Microporous Solids. A Wiley-Interscience Pubs., New York.

Leong, K.C., Liu, Y., 2004. Numerical modeling of combined heat and mass transfer in the adsorbent bed of a zeolite/water cooling system. Appl. Therm. Eng. 24, 2359–2374.

Li, M., Wang, R.Z., 2003. Heat and mass transfer in a flat plate solar solid adsorption refrigeration ice maker. Renew. Energ. 28, 613–622.

Maggio, G., Freni, A., Restuccia, G., 2006. A dynamic model of heat and mass transfer in a double-bed adsorption machine with internal heat recovery. Int. J. Refrig. 29, 589–600.

Marletta, L., Maggio, G., Freni, A., Ingrasciotta, M., Restuccia, G., 2002. A non-uniform temperature non-uniform pressure dynamic model of heat and mass transfer in compact adsorbent beds. Int. J. Heat Mass Tran. 45, 3321–3330.

Mhimid, A., 1998. Theoretical study of heat and mass transfer in a zeolite bed during water desorption: validity of local thermal equilibrium assumption. Int. J. Heat Mass Tran. 41, 2967–2977.

Nield, D.A., Bejan, A., 1999. Convection in Porous Media, second ed. Springer.

Rady, M.A., Huzayyin, A.S., Arquis, E., Monneyron, P., Lebot, C., 2008. Heat and Mass Transfer in a Composite Bed of Silica Gel and Macro-encapsulated Pcm for Dehumidification. 5th European Thermal-Sciences Conference, Netherlands.

Sözen, M., Vafai, K., 1990. Analysis of the non-thermal equilibrium condensing flow of a gas through a packed bed. Int. J. Heat Mass Tran. 33, 1247–1261.

Wu, W.D., Zhang, H., Sun, D.W., 2009. Mathematical simulation and experimental study of a modified zeolite 13X-water adsorption refrigeration module. Appl. Therm. Eng. 29, 645–651.

Zhang, L.Z., Wang, L., 1999. Effects of coupled heat and mass transfers in adsorbent on the performance of a waste heat adsorption cooling unit. Appl. Therm. Eng. 19, 195–215.

Zhang, L.Z., 2000. A three dimensional non-equilibrium model for an intermittent adsorption cooling system. Solar Energy 69, 27–35.